Effect of endothelial cell heterogeneity on nanoparticle uptake

Aldy Aliyandi[1], Simon Satchell[2], Ronald E. Unger[3], Birke Bartosch[4], Romain Parent[4], Inge S. Zuhorn[5], and Anna Salvati[1*]*

[1] Department of Nanomedicine & Drug Targeting, Groningen Research Institute of Pharmacy, University of Groningen, Antonius Deusinglaan 1, 9713AV Groningen, The Netherlands (email address: AA a.aliyandi@rug.nl; AS a.salvati@rug.nl)

[2]Bristol Renal, University of Bristol, Dorothy Hodgkin Building, Whitson Street, BS1 3NY Bristol, England (email address: s.c.satchell@bristol.ac.uk)

[3]Institute of Pathology, REPAIR-Lab, Johannes Gutenberg University, Langenbeckstr. 1, 55101 Mainz, Germany (email address: runger@uni-mainz.de)

[4]INSERM, Lyon Cancer Research Center, 28 Rue Laennec, 69008 Lyon, France (email address: RP romain.parent@inserm.fr; BB birke.bartosch@inserm.fr)

[5]Department of Biomedical Engineering, University of Groningen, University Medical Center Groningen, Antonius Deusinglaan 1, 9713AV Groningen, The Netherlands (email address: i.zuhorn@umcg.nl)

[*] Corresponding authors:
Department of Nanomedicine & Drug Targeting, Groningen Research Institute of Pharmacy, University of Groningen, Antonius Deusinglaan 1, 9713AV Groningen, The Netherlands
Email address: a.salvati@rug.nl
Tel: +31 50 363 9831/3272; Fax: +31 50 3633247

Department of Biomedical Engineering, University of Groningen, University Medical Center Groningen, Antonius Deusinglaan 1, 9713AV Groningen, The Netherlands
Email address: i.zuhorn@umcg.nl

The authors declare no conflicts of interest

Abstract

Endothelial cells exhibit distinct properties in morphology and functions in different organs that can be exploited for nanomedicine targeting. In this work, endothelial cells from different organs, i.e. brain, lung, liver, and kidney, were exposed to plain, carboxylated, and amino-modified silica. As expected, different protein coronas were formed on the different nanoparticle types and these changed when foetal bovine serum (FBS) or human serum were used. Uptake efficiencies differed strongly in the different endothelia, confirming that the cells retained some of their organ-specific differences. However, all endothelia showed higher uptake for the amino-modified silica in FBS, but, interestingly, this changed to the carboxylated silica when human serum was used, confirming that differences in the protein corona affect uptake preferences by cells. Thus, uptake rates of fluid phase markers and transferrin were determined in liver and brain endothelia to compare their endocytic activity. Overall, our results showed that endothelial cells of different organs have very different nanoparticle uptake efficiency, likely due to differences in receptor expression, affinity, and activity. A thorough characterization of phenotypic differences in the endothelia lining different organs is key to the development of targeted nanomedicine.

1. Introduction

Nano-sized materials hold tremendous potential as drug carriers, thanks to their ability to distribute within organisms and enter cells (Bareford and Swaan, 2007; Ferrari, 2005; Peer et al., 2007; Sahay et al., 2010). Although their use as carriers of therapeutic agents has been growing rapidly during the past decades, crucial questions still arise as to how nanoparticles can be effectively and selectively delivered to their target. In order to reach their target tissue, following administration into the bloodstream, nano-sized drug carriers, in most cases, first need to interact with and cross endothelial cell barriers. Due to the diversity in vascular channels and other associated differences — for instance, in hemodynamics and their embryonic origin

— endothelial cells lining blood vessels of different organs exhibit very distinct properties in morphology and functions (Aird, 2012; Chi et al., 2003; Ribatti et al., 2002). Consequently, these differences provide a great opportunity to selectively target drug carriers to specific endothelial cell barriers (Ding et al., 2006; Kowalski et al., 2013; Muro et al., 2008; Simone et al., 2009).

To date, most efforts in nanomedicine targeting have been devoted to understanding the effect of different physicochemical properties of nanoparticles and the environment in which they are applied on their interaction with cells. Several nanoparticles properties such as the size (Chithrani et al., 2006; He et al., 2010; Rejman et al., 2004), shape (Chithrani et al., 2006), surface charge (Arvizo et al., 2010; He et al., 2010), and (core) materials (Georgieva et al., 2011), as well as environmental properties such as protein composition of the biological fluids in which they are dispersed (Lesniak et al., 2012), pH (Shen et al., 2008), temperature, flow (Freese et al., 2017) and shear stress (Klingberg et al., 2015) have been shown to have a significant influence on nanoparticle-cell interactions. However, relatively less attention has been paid on differences in cellular properties, which can affect nanoparticle-cell interactions. For instance, we have previously shown that a specific cell type can show very different nanoparticle uptake behavior when it is developed into a polarized cell monolayer, i.e., a cell barrier, as opposed to confluent cells (Francia et al., 2018; Zuhorn et al., 2007). The development of cells into cell barriers reduced the gene expression levels of different protein markers and/or caused their relocation to the abluminal plasma membrane, resulting in lower uptake efficiency of luminally applied nanoparticles. It is known that polarized cell barriers express different uptake pathways and receptors on their apical and basal side, and this can affect nanoparticle uptake (Georgieva et al., 2011; Iversen et al., 2011; Wang et al., 2016). Similarly, because of their phenotypical heterogeneity, endothelial cells of different tissue origins are likely to show very different nanoparticle uptake behavior, and this could be

exploited for nanomedicine targeting. As an example, a recent study showed that kidney glomerulus and blood-brain barrier had a distinct nanoparticle uptake behavior (Gromnicova et al., 2016). In addition to a different origin, heterogeneity induced by physiological stress can also lead to the expression of different proteins on endothelial cells, and these have been shown to be excellent targets for drug carriers (Ding et al., 2006; Kowalski et al., 2013, 2011).

The aim of this study was to investigate the cellular uptake behavior of nanoparticles on endothelial barriers generated from endothelial cells derived from different organs. We hypothesized that different endothelia would show preferential uptake for certain types of nanoparticles, and similar differences could be exploited for targeting. To test this hypothesis, four endothelial cell lines derived from different organs were chosen as endothelial cell models: hCMEC/D3 (brain), HPMEC-ST1.6R (lung), TRP3 (liver), and ciGENC (kidney). The selection of these organs was based on the high phenotypic differences between one another. In addition, the selected immortalized endothelial cell lines have been shown to be excellent models of the endothelia of the respective organ from which they were derived, since they retained their organ-specific properties *in vitro*.(Krump-Konvalinkova et al., 2001; Parent et al., 2014; Satchell et al., 2006; Weksler et al., 2005) The exhibition of organ-specific characteristics of the cell lines *in vitro* was essential for this comparative study. Amorphous silica nanoparticles of 100 nm with three different surface functionalizations, plain, carboxylated and amino-modified, were used as representative model nanoparticles. It is known that surface properties affect corona formation on the nanoparticles in serum and this, in turn, affects nanoparticle recognition by cell receptors and uptake by cells (Caracciolo et al., 2017, 2013; Francia et al., 2019; Lara et al., 2017; Lundqvist et al., 2008; Ritz et al., 2015; Tenzer et al., 2013). We hypothesized that due to varying coronas, the different nanoparticles would naturally target specific organ endothelia. Therefore, cell culture conditions were optimized to develop endothelial cell barriers and uptake kinetics of the various nanoparticles were compared

in the organ-specific endothelia in order to determine differences in uptake behavior. Finally, the rate of endocytosis of fluid phase markers and transferrin in the blood brain barrier and the liver sinusoids were compared in order to identify potential differences which may account for different uptake efficiency of nanoparticles in these cells.

2. Methods

2.1 Cell culture

The immortalized human brain endothelial cell line, hCMEC/D3, was supplied by Pierre-Olivier Couraud (Weksler et al., 2005). Cells were cultured in standard cell culture flasks pre-coated with 0.1 mg/ml cold rat-tail collagen type-I (Corning, NY, USA) in an endothelial basal medium (EBM-2, LONZA, Allendale, NJ, USA) supplemented with 5% fetal bovine serum (FBS, Gibco Thermofisher Scientific, Landsmeer, Netherlands), 200 ng/ml bFGF (Peprotech, London, United Kingdom), 1 µg/ml hydrocortisone (Sigma-Aldrich, St Luis, USA), 1% chemically defined lipid concentrate (Thermofisher Scientific), and 10 mM HEPES (Thermofisher Scientific). The medium was refreshed every 2-3 days, and cells were cultured between passages 29-38. Cells were kept under standard conditions (37˚C, 5% CO_2).

The immortalized human pulmonary microvascular endothelial cell line, HPMEC-ST1.6R, was supplied by Ronald E. Unger (Krump-Konvalinkova et al., 2001). Cells were cultured in standard cell culture flasks pre-coated with 0.2% cold gelatin (Sigma-Aldrich) in an EBM-2 supplemented with an EGM-2 bullet kit (LONZA). The medium was refreshed every 2-3 days, and cells were kept under standard conditions (37˚C, 5% CO_2).

The immortalized human liver endothelial sinusoidal cell line, TRP3, was supplied by Birke Bartosch and Romain Parent (Parent et al., 2014). Cells were cultured in standard cell culture flasks pre-coated with 0.1% cold gelatin (Sigma-Aldrich) in an MCDB 131 medium (Gibco Thermofisher Scientific) supplemented with 20% FBS (Gibco Thermofisher Scientific), 10 mM

glutamine (Thermofisher Scientific), 250 µg/ml cAMP (Sigma-Aldrich),1 µg/ml hydrocortisone (Sigma-Aldrich), and 50 µg/ml endothelial cell growth supplement (ECGS, Corning). The medium was refreshed every 2-3 days, and cells were kept under standard conditions (37˚C, 5% CO_2).

The conditionally immortalized glomerular endothelial cell line, CiGENC, was supplied by Simon Satchell (Satchell et al., 2006). Cells were cultured in standard cell culture flasks pre-coated with 1 µg/cm^2 fibronectin (Corning) in an EBM-2MV supplemented with an EGM-2MV bullet kit (LONZA), with the exception of VEGF, which was not added to the medium. The medium was refreshed every 2-3 days. Cells were kept at 33˚C with 5% CO_2 until they were 90% confluent.

2.2 Endothelial cell barrier formation

An endothelial cell barrier with each cell line was obtained by seeding 25,000 cells/cm^2 for HPMEC-ST1.6R, or 50,000 cells/cm^2 for the other cell lines, respectively, in a 24-well plate (Corning) pre-coated as described above. The cells were cultured for an additional three days for ciGENC and TRP3, or four days for hCMEC/D3 and HPMEC-ST1.6R, respectively, and kept under standard conditions (37˚C, 5% CO_2). The medium was refreshed every two days.

2.3 Immunohistochemistry

Cell confluency and morphology were assessed by light microscopy (Olympus IX50). For immunohistochemistry, 25000 cells/cm^2 for HPMEC-ST1.6R or 50000 cells/cm^2 for the other cell lines, respectively, were seeded in a 24-well plate (Corning) on glass coverslips pre-coated as described above for each cell line. Three days after seeding, for ciGENC and TRP3, or four days for hCMEC/D3 and HPMEC-ST1.6R, respectively, cells were fixed with formaldehyde (4% v/v) solution for 15 minutes and then permeabilized with Triton X-100 (0.1% v/v) for 5 minutes. Then, cells were incubated with an antibody against the tight junction proteins zonula

occludens-1 (ZO-1, Life technologies, NY, USA) and CD31 (also known as platelet endothelial cell adhesion molecule, PECAM1, Dako, Glostrup, Denmark) for 1 hour at room temperature, followed by incubation with Alexa Fluor 488- (Life Technologies, NY, USA) and Cy5- labelled (Jackson Immuno Research Laboratories, Inc., PA, USA) secondary antibodies for 1 hour. Nuclear staining was performed by incubating cells for 5 minutes with 0.2 ug/ml 4',6-diamidino-2-phenylindole (DAPI). Afterwards, slides were mounted with Mowiol 4-88 mounting medium (EMD Chemical, Inc., CA, USA). Fluorescence imaging was performed using a Leica TCS SP8 confocal fluorescence microscope (Leica Microsystems, Wetzlar, Germany) with a 405 nm laser for DAPI excitation, a 488 nm laser for Alexa Fluor 488, and 638 nm laser for Cy5. Images were processed using ImageJ software (http://www.fiji.sc). Brightness was adjusted to improve visualization.

2.4 Nanoparticle characterization

Green fluorescently labeled (maximum excitation and emission wavelength 485 and 510 nm, respectively) plain (non-functionalized, SiO_2), amino-modified (SiO_2-NH_2), and carboxylated silica nanoparticles (SiO_2-COOH) of 100 nm were purchased from Micromod Partikeltechnologie GmbH (Rostock, Germany). Nanoparticle size distribution by dynamic light scattering (DLS) and zeta potential (ζ-potential) were measured using a Malvern Zetasizer Nano ZS (Malvern Instrument Ltd., Worcestershire, UK). Briefly, nanoparticles (100 µg/ml) were dispersed in PBS, dH_2O or cell culture medium supplemented with 5 mg/ml FBS (Gibco Thermofisher Scientific), corresponding to the standard 10% v/v cell culture medium, or the same amount of human serum (human serum from pooled donors, from TCS BioSciences Ltd Botolph Claydon, Buckingham, UK). Samples were measured at 20˚C immediately, or after 24-hour incubation at 37˚C using disposable capillary cells (Malvern). The results are the average of 5 runs of at least 3 measurements.

2.5 Nanoparticle uptake and flow cytometry analysis

Cell fluorescence intensity was used as a measurement of nanoparticle uptake on the endothelial cell barriers. Briefly, after developing cell barriers as described above, cells were exposed for 1, 3, 5, 24, and 26 hours to 50 µg/ml SiO_2, SiO_2-NH_2, or SiO_2-COOH. Nanoparticles were dispersed at room temperature in cell culture medium containing 5 mg/ml FBS (Gibco Thermofisher Scientific) or human serum (TCS BioSciences). Cells were exposed to the freshly prepared nanoparticle dispersions immediately after mixing by replacing the cell culture medium. After exposure, in order to remove the excess of nanoparticles and reduce the presence of nanoparticles adhering outside the cell membrane which could interfere with uptake quantification, cells were washed once with cell culture medium supplemented with 10% FBS (Gibco Thermofisher Scientific) and twice with PBS. Afterwards, cells were detached using 0.05% trypsin-EDTA. Cell fluorescence was measured using a Cytoflex S Flow Cytometer (Beckman Coulter, Woerden, The Netherlands) with a 488 nm laser. Data were analyzed by Flowjo data analysis software (Flowjo, LLC). Dead cells and cell doublets were excluded from the plots by setting gates in the forward and side scattering double scatter plots. At least 15,000 cells were acquired per sample, and the median of the obtained cell fluorescence distribution calculated. For each exposure time, duplicate samples were made and their median cell fluorescence intensity is shown, together with their average. The results of an independent replicate experiment are shown in Supplementary Figures S2-3 to confirm the trends observed.

2.6 Nanoparticle-corona formation and characterization

In order to examine the corona formed on the different nanoparticles, 1 mg/ml SiO_2, SiO_2-NH_2, or SiO_2-COOH of 100 nm size were dispersed in PBS containing 5 mg/ml FBS (Gibco Thermofisher Scientific) or human serum (TCS BioSciences) and incubated at 37˚C under continuous shaking at 300 rpm for 1 hour. After this, the dispersion was centrifuged for 1 hour at 16,000 g in order to pellet the corona-coated nanoparticles. The pellet was washed in PBS

and centrifuged again for 1 hour at 16,000 g for a total of three centrifugations to remove the soft serum corona and excess free proteins in solutions and isolate hard corona-coated nanoparticles. The final amount of nanoparticles present in the pellet was quantified by measuring their fluorescence with a spectrofluorometer. Afterwards, 200 µg hard corona-coated nanoparticles were resuspended in gel loading buffer, boiled for 5 minutes at 95˚C, and loaded onto 10% polyacrylamide gel for SDS-PAGE. After electrophoresis, the gel was incubated for 1 hour with a solution containing 0.1% w/v Coomassie blue R-250 in a water : methanol : glacial acetic acid (5:4:1) solution and washed with milliQ water. Pictures were taken with a ChemiDoc XRS (Biorad, USA). After this, the intensity of selected bands was quantified using ImageJ software (http://www.fiji.sc) to evaluate differences in the isolated coronas.

2.7 mRNA expression of transferrin

The expression level of transferrin receptor genes TFR1 and TFR2 in brain and liver endothelia was determined by RT-PCR. TRP3 or hCMEC/D3 cells were cultured to form a cell barrier as described above. Then, total mRNA was isolated with a Maxwell instrument and Maxwell 16 LEV simplyRNA Cells Kit (Promega, Madison, WI, USA) according to the instructions provided by the manufacturer. Reverse transcription of mRNA into cDNA was performed with a Reverse Transcription System (Promega, Leiden, The Netherlands) in an Eppendorf Mastercycler gradient (the following cycle was used: 20˚C for 10 min, 42˚C for 30 min, 20˚C for 12 min, 99˚C for 5 min and 20˚C for 5 min). The transcription levels were measured by quantitative real-time PCR (SensiMix SYBR kit, Bioline, Taunton, MA, USA) in an ABI7900HT sequence detection system (Applied Biosystems, Foster City, CA, USA) from cDNA (10 ng per sample). The Ct values were obtained with the SDS 2.4 software (Applied Biosystems). For each target, four replicates were used, and the average Ct value and its standard deviation were calculated. Results are expressed as fold-change of the averaged Ct values of TRP3 (Ct_{TRP3}) related to Ct values of hCMEC/D3 (Ct_{D3}) as follows:

$$\text{Fold change} = 2^{-(\text{Mean } Ct_{TRP3} - \text{Mean } Ct_{D3})}.$$

2.8 Analysis of the rate of endocytosis

The rate of endocytosis in brain and liver endothelia was determined using dextran as a fluid-phase marker and transferrin as an example of a molecule that follows the route of receptor-mediated endocytosis. TRP3 and hCMEC/D3 cells were cultured to form a cell barrier as described above. Then, cells were incubated for different time periods with 250 µg/ml TRITC dextran 10 kDa (Life technologies, NY, USA) dispersed in cell culture medium or with 10 µg/ml Alexa Fluor 546 fluorescently labeled transferrin (Life Technologies, NY, USA) dispersed in serum-free medium. Prior to incubation with transferrin, cells were pre-incubated with serum-free medium for 20 minutes. After exposure, cells were harvested and analyzed by flow cytometry as described above with a 488 nm and 561 nm laser. At least 15,000 cells were acquired per sample, and the median of the obtained cell fluorescence distribution calculated. For each exposure time, duplicate samples were made and their median cell fluorescence intensity is shown, together with their average. The results of an independent replicate experiment are shown in Supplementary Figure S5 to confirm the trends observed.

2.9 Statistical analysis

For nanoparticle uptake and rate of endocytosis studies, linear regression two-tailed Student's t-test was used as a simple approximation to compare the uptake kinetics between different samples. For DLS results, an unpaired two-tailed Student's t-test was used to determine statistically significant differences in the average nanoparticle hydrodynamic diameter after dispersion in serum in comparison to the results in PBS. In addition, for qPCR, an unpaired two-tailed Student's t-test was used to determine statistically significant differences in expression levels in TRP3 cells in comparison to the results in hCMEC/D3. A p value <0.01 or <0.05 was considered statistically significant. Differences are not labelled if not significant.

3. Results

3.1 Endothelial cell barrier characterization

Prior to nanoparticle uptake studies, cell culture conditions were optimized to ensure a proper formation of cell barriers. Four immortalized endothelial cell lines derived from different organs were selected as cell models: hCMEC/D3 (brain), HPMEC-ST1.6R (lung), TRP3 (liver), and ciGENC (kidney). To confirm cell barrier formation, the expression and cellular distribution of ZO-1, a tight junction protein, and CD31, an adhesion protein that is enriched at the basolateral surface of polarized endothelial cell monolayers, were assessed using confocal microscopy. As shown in Figure 1A-D, cell monolayers derived from all four cell lines showed a lateral localization of ZO-1 and CD31, indicating the development of a cell barrier. Interestingly, each cell line also showed a unique cell shape and barrier morphology (Figures 1A-D, left), which suggested that the different endothelia retained at least in part some of their organ-specific properties (Krump-Konvalinkova et al., 2001; Parent et al., 2014; Satchell et al., 2006; Weksler et al., 2005).

3.2 Nanoparticle physicochemical characterization

Green-labeled 100 nm silica nanoparticles with three different surface functionalizations (SiO_2, SiO_2-NH_2, and SiO_2-COOH) were selected as nanoparticle models with varying surface properties to form different coronas and test uptake preferences in the different endothelial barriers. For exposure to cells, the nanoparticles were dispersed in their respective cell culture media supplemented with 5 mg/ml FBs or human serum. Dynamic light scattering (DLS) was used to characterize the stability of the nanoparticle dispersions under these conditions. The results confirmed that stable dispersions were obtained for all nanoparticles (Table 1 and Figure 2). The observed increase in hydrodynamic diameter of nanoparticles when incubated in medium containing FBS or human serum confirmed protein adsorption on the surface of nanoparticles and corona formation.

In addition to the hydrodynamic diameter, the zeta potential of the nanoparticles was characterized. As expected, plain (SiO_2) and carboxylated (SiO_2-COOH) silica nanoparticles showed negative zeta potential when dispersed in water or PBS (Table 1). For the amino-modified silica nanoparticles (SiO_2-NH_2), a negative zeta potential in water and PBS was also observed. These nanoparticles show a positive zeta potential only at pH below 3.5 (data from the manufacturer). As expected (Lesniak et al., 2012; Monopoli et al., 2011), all the nanoparticles showed near-neutral zeta potential when incubated in a medium containing FBS or human serum, regardless of their surface functionalization (Table 1), as a consequence of protein adsorption and corona formation on the surface of nanoparticles. Despite the decrease in zeta potential absolute value towards neutrality, nanoparticle dispersions remained stable, likely due to the steric stabilization by the adsorbed proteins. SDS-PAGE was then used to identify the corona proteins on the different nanoparticles (Supplementary Figure S1). Quantification of the intensity of selected bands confirmed different coronas were formed, as expected due to the different functionalization. However, the banding pattern was relatively similar across the different samples.

3.3 Nanoparticle uptake by human endothelial barriers from different organs

We next investigated the cellular uptake kinetics of the silica nanoparticles in the endothelial cell barriers of different organs in order to determine whether there was preferential uptake of certain types of nanoparticles by specific endothelial cell types. In addition, we also investigated whether the uptake was different when the nanoparticles were dispersed in different types of serum, bovine or human. It is known that dispersions in different sera can lead to the formation of different coronas (Francia et al., 2019; Monopoli et al., 2011; Partikel et al., 2019). SDS-PAGE of the corona proteins isolated from the surface of the nanoparticles after incubation with either FBS or human serum shows differences in the banding patterns (molecular weight and

intensity), confirming that different coronas were formed when nanoparticles were dispersed in different sera (Supplementary Figure S1).

Figures 3 and 4 clearly show that nanoparticle uptake efficiency was different in each barrier culture, confirming that, even when cultured *in vitro*, these cells retain at least in part some of the different cellular properties of the organs from which they originated (Figures 3 and 4 for experiments in bovine or human serum, respectively and Supplementary Figures S2-3 for the results obtained in independent replicate experiments). When incubated in FBS, nanoparticles accumulated at the highest level in kidney and liver endothelia, followed by lung endothelium, and the lowest accumulation was observed in the cells from the blood-brain barrier (Figure 3). Similar results were also observed when human serum was used, but with closer uptake levels in liver and lung endothelia, than in kidney (Figure 4). In addition, the overall uptake efficiency for all nanoparticles in all barrier cultures was lower when nanoparticles were incubated in human serum, indicating that the serum source also clearly influenced uptake. Similar effects were previously observed (Francia et al., 2019; Salvati et al., 2013). After this, as a simple approximation, linear fit and statistical analysis were applied to compare the uptake kinetics of the different nanoparticles for each cell line (see Section 2.9 for details). No differences were observed between the different endothelial cell barriers concerning the relative uptake efficiencies of the different nanoparticles (Figures 3 and 4). Specifically, statistical analysis confirmed that all cell lines showed higher uptake for SiO_2-NH_2 when dispersed in FBS (Figure 3), while a higher uptake for SiO_2-COOH was observed when nanoparticles were dispersed in human serum. However, this latter was statistically significant only in the case of the brain endothelial cells (Figure 4A). This indicated that changing corona composition by dispersion in different sera can affect nanoparticle uptake preference. Similar trends were observed in independent replicate experiments (Supplementary Figures S2-3). Additionally, we performed equivalent studies using another nanoparticle type, namely liposomes of around 100 nm, and

compared uptake of negatively-charged DOPG liposomes and zwitterionic DOPC in brain and liver endothelium, both in FBS and in human serum (Supplementary Figure S4). The zwitterionic liposomes are known to adsorb lower amounts of protein in serum and show lower uptake than charged ones (Yang et al., 2020). In line with this, we found that, in both endothelia, the uptake kinetics of the two formulations differed, and in all conditions, in the first hours of exposure, the negatively-charged DOPG liposomes showed significantly higher uptake in comparison to the zwitterionic DOPC liposomes, later converging to comparable levels (Supplementary Figure S4). Additionally, as also observed with the silica nanoparticles, in all cases, uptake was higher when the liposomes were added to cells in mediun with FBS than with HS and uptake was higher in liver than in brain endothelium, the effect being more evident for liposomes dispersed in FBS.

3.4 Rate of endocytosis of brain and liver endothelia

As a final step, we investigated whether the observed differences in nanoparticle uptake efficiency between the different barrier cultures could be due to differences in their rate of endocytosis. For this purpose, we used brain and liver endothelia, which showed the lowest and highest nanoparticle uptake, respectively. The rate of endocytosis was determined by using FITC-dextran 10 kDa as a fluid-phase marker, and transferrin, as an example of a protein which is internalized via receptor-mediated endocytosis. Uptake kinetics were determined and linear fit applied to statistically compare the trend of uptake rates (see Section 2.9 for details, Figure 5 and Supplementary Figure S5 for the results obtained in independent replicate experiments). As shown in Figure 5A, there was no major difference in the uptake rate of FITC-dextran. However, the liver endothelium showed much higher transferrin uptake in comparison to brain endothelium (Figure 5B). We then investigated whether this was due to a higher expression level of the transferrin receptor TFR1. Interestingly, as shown in Figure 5C, we found that the liver endothelium had 2.5 times lower expression of TFR1 compared to the brain endothelium.

However, the expression level of the secondary transferrin receptor TFR2 was shown to be three times higher in liver endothelium, possibly explaining the higher transferrin uptake in the liver. Overall, these results confirmed that different endothelial cells express cell receptors to different levels and show differences in uptake rates.

4. Discussion

The aim of this study was to investigate the effect of endothelial cell heterogeneity on the cellular uptake of nanoparticles. More specifically, we aimed to determine whether by changing nanoparticle properties, thus forming different coronas nanoparticles could be targeted to specific organs. Previously it has been shown that changing nanoparticle size, charge, or other similar parameters can affect nanoparticle distribution *in vivo*. This may be related to differences in the type of corona formed and may confer "natural targeting" to organ-specific endothelial cells (De Jong et al., 2008; He et al., 2010; Hirn et al., 2011). These effects could be exploited for nanomedicine targeting (Blanco et al., 2015). To determine whether this could be possible, we chose four unique organ-derived endothelial cell lines: hCMEC/D3 (blood-brain barrier), HPMEC-ST1.6R (lung microvasculature), TRP3 (liver sinusoid), and ciGENC (kidney glomerulus). These endothelial cell lines are well characterized immortalized cell lines and retain many of their organ-specific properties (Krump-Konvalinkova et al., 2001; Parent et al., 2014; Satchell et al., 2006; Weksler et al., 2005). Endothelial cell barriers were formed and exposed to silica nanoparticles with three different surface functionalizations in the presence of bovine or human serum. Silica nanoparticles, in general, are well characterized and are known to form stable dispersions in cell medium supplemented with proteins (Lesniak et al., 2012; Monopoli et al., 2011; Shapero et al., 2011). Several studies have reported that surface charge (among many other nanoparticle properties) affects corona formation and nanoparticle uptake into specific cell types (Arvizo et al., 2010; Chithrani et al., 2006; He et al., 2010; Rejman et al., 2004). Thus, here silica nanoparticles with different surface functionalization were used as

a model system to form different coronas and test potential differences in uptake preferences across the different cell types. As expected due to the different surface functionalization, quantification of the bands obtianed by SDS-PAGE on the proteins recovered from the three nanoparticles confirmed that different coronas were formed (Supplementary Figure S1).

Flow cytometry was used to measure nanoparticle uptake by cells. Protocols were optimized to reduce the eventual presence of nanoparticles remaining outside of the cells (see Section 2.5 for details). Additionally, uptake was measured at multiple time points to determine uptake kinetics and compare their rate (this also allows to exclude eventual contribution of residual nanoparticles adhering outside cells (Lesniak et al., 2013)). As previously observed, uptake levels were much lower in human serum than in FBS, likely due to higher competition for cell receptors between the nanoparticles and free ligands in serum when human instead of bovine serum was used on the human cells, as well as differences in corona compostion in the different sera (Supplementary Figure S1) (Francia et al., 2019). When the uptake of the different nanoparticle types for each cell type was compared, uptake levels were different. Thus, despite having the same size and similar zeta potential after dispersion in serum (Table 1 and Figure 2), the three nanoparticles were taken up by cells at different levels, as expected because of their different functionalization and corona (Supplementary Figure S1). However, the three nanoparticles were taken up by the various endothelial barrier models following similar trends: in fact, it was found that for all cell types, when the nanoparticles were dispersed in FBS, the uptake was higher for SiO_2-NH_2 (also confirmed by statistical analysis on the uptake rates, see Figure 3). For nanoparticles in human serum, however, a higher uptake was observed for SiO_2-COOH and the effect was only statistically significant in the brain endothelium (Figure 4). A possible interpretation of the similar uptake preferences among the different types of endothelial cells is that the degree of functionalization of these nanoparticles was not very high. It will be interesting to perform similar studies for nanoparticles with a higher degree of

functionalization to study in detail how the degree of functionalization affects the nanoparticle corona, thus also uptake by cells. Nevertheless, uptake preferences changed dramatically when the nanoparticles were incubated with either FBS or human serum. It is known that corona proteins can mediate recognition and interaction of nanoparticles with cell receptors (Francia et al., 2020, 2019; Lara et al., 2018, 2017; Nel et al., 2009; Salvati et al., 2013). Thus, the different uptake preferences observed are likely due to differences in the protein corona composition on the nanoparticles when incubated with FBS or human serum (as indeed we show in Supplementary Figure S1). This supports the overall hypothesis that tuning the corona composition on a nanoparticle (for instance by changing nanomaterial properties such as size, charge, composition or by pre-forming artificial coronas) can be used as a strategy to modulate uptake preferences in different cell types, thus potentially allowing a preferential targeting of nanoparticles to specific organs *in vivo*. Additionally the results from our studies have shown that even small changes in a single type of nanoparticle can affect its uptake in endothelial cells from different locations in the body. These studies indicate that much needs to be done to determine how and if size, shape, chemical composition etc. influence the uptake of nanoparticles. Nanoparticles of different size or material could also be used to form different coronas and test similar effects, as indeed we observed here using liposomes of different charge (Supplementary Figure S4). Another important observation is that despite the similar uptake preferences observed by certain types of nanoparticles, nanoparticle uptake efficiency differed strongly in the different endothelial barrier models. Thus, in agreement with common observations for *in vivo* distribution studies with silica and other nanoparticles, kidney and liver endothelia showed a higher uptake, possibly related to the physiological role of these organs in excretion (De Jong et al., 2008; Gromnicova et al., 2016; Waegeneers et al., 2018; Wilhelm et al., 2016). In contrast, the blood-brain barrier, known to be the tightest of the endothelial barriers (Abbott et al., 2010; Ballabh et al., 2004), showed the lowest uptake efficiency for the

nanoparticles. In agreement with this, lower nanoparticle uptake in the brain is also commonly observed *in vivo* (De Jong et al., 2008; Gromnicova et al., 2016; Semete et al., 2010). Similar results were observed by Gromnicova et al., who showed that the internalization of gold nanoparticles was significantly higher in kidney than in brain endothelium (Gromnicova et al., 2016). The differences in uptake efficiency could also be a reflection of differences in their rate of endocytosis. In line with this, we showed that while the rate of endocytosis of a fluid-phase marker (FITC-dextran 10 kDa) in liver and brain endothelium was comparable, the uptake of transferrin, here selected as an example to compare the rate of a receptor-mediated uptake in the two cell types, was much higher in the liver (Figure 5). Since corona-coated nanoparticles are known to be internalized via active processes, and in several cases, it has been shown that uptake occurs after interaction with cell receptors (Francia et al., 2020; Lara et al., 2018, 2017), the higher nanoparticle uptake in liver endothelium in comparison with brain endothelium is likely connected to similar differences in receptor activity among the different endothelia. Interestingly, the uptake rate of transferrin and the expression level of transferrin receptor TFR1 were inversely related between liver and brain endothelium. Since TFR1 is known to be the main receptor for transferrin, it is possible that despite the lower expression level in liver endothelium, this receptor is recycled faster in liver endothelium than in brain endothelium. In addition, the higher expression level of the secondary transferrin receptor TFR2 in liver endothelium could also contribute to the higher uptake of transferrin. These results suggest that differences in receptor expression and activity, rather than the basal rate of (fluid-phase) endocytosis, may potentially determine the differences observed in the uptake efficiency of nanoparticles. Thus, it would be interesting to identify the receptors involved in the uptake of these specific nanoparticles and compare their expression and activity in the different cell types. It is also important to note that in order to use the same protein content for corona formation, the nanoparticle dispersions were prepared with the same type and amount of sera for all

endothelia, but using different basal media, as required for each cell type. Previous studies have shown that even when using the same serum and nanoparticles, the use of different cell culture media could affect protein corona formation, and, consequently, uptake by cells (Maiorano et al., 2010; Strojan et al., 2017). However, here, three out of the four endothelia (brain, lung and kidney endothelia) were cultured using the same basal media and only some supplements differed. Thus, the observed uptake differences were most likely due to the heterogeneity of each endothelia, rather than these subtle differences in the media. More importantly, the different endothelial barrier models showed differences in uptake efficiency, which reflected the different physiological functions of the various organs from which they originated. These results suggested that the *in vitro* models generated with the different cell lines retained a high degree of the distinctive features present in the endothelia of the organ type.

5. Conclusion

The results from the present study confirm that the heterogeneity of endothelial cells clearly influences the uptake of nanoparticles by different organs. Since most drugs lack specificity for endothelial cells, the ability to effectively target specific endothelial cells using nanoparticles could offer significant benefits for future clinical applications. Our findings highlight the importance of exploiting further endothelial cell heterogeneity for better design of targeted drug carriers. Identification of relevant receptors to enable selective uptake by specific endothelial cell types may provide valuable information for improving the design of such carriers. In addition to the genotypic and phenotypic profiling of endothelial cell types, the identification of relevant receptors for targeted nanomedicine may be deduced from the protein corona composition of nanoparticles that show preferential interaction with the cell type of choice (Bewersdorff et al., 2017).

Acknowledgements

Pierre-Olivier Couraud (Institute Cochin) is acknowledged for providing hCMEC/D3. Ingrid Molema and Henk Moorlag (Endothelial Biomedicine & Vascular Drug Targeting, UMCG) are acknowledged for the useful discussions on endothelial cell models and the support with the ciGENC cell culture. Edwin de Jong is acknowledged for the support with hCMEC/D3 cell culture. This work was partially funded by the European Research Council (Grant agreement: N °637614). A. S. kindly acknowledges the University of Groningen for additional funding (Rosalind Franklin Fellowship).

References

Abbott, N.J., Patabendige, A.A.K., Dolman, D.E.M., Yusof, S.R., Begley, D.J., 2010. Structure and function of the blood-brain barrier. Neurobiol. Dis. https://doi.org/10.1016/j.nbd.2009.07.030

Aird, W.C., 2012. Endothelial cell heterogeneity. Cold Spring Harb. Perspect. Med. 2, a006429–a006429. https://doi.org/10.1101/cshperspect.a006429

Arvizo, R.R., Miranda, O.R., Thompson, M.A., Pabelick, C.M., Bhattacharya, R., Robertson, J.D., Rotello, V.M., Prakash, Y.S., Mukherjee, P., 2010. Effect of Nanoparticle Surface Charge at the Plasma Membrane and Beyond. Nano Lett. 10, 2543–2548. https://doi.org/10.1021/nl101140t

Ballabh, P., Braun, A., Nedergaard, M., 2004. The blood-brain barrier: An overview: Structure, regulation, and clinical implications. Neurobiol. Dis. https://doi.org/10.1016/j.nbd.2003.12.016

Bareford, L., Swaan, P., 2007. Endocytic mechanisms for targeted drug delivery☆. Adv. Drug Deliv. Rev. 59, 748–758. https://doi.org/10.1016/j.addr.2007.06.008

Bewersdorff, T., Vonnemann, J., Kanik, A., Haag, R., Haase, A., 2017. The influence of surface charge on serum protein interaction and cellular uptake: studies with dendritic polyglycerols and dendritic polyglycerol-coated gold nanoparticles. Int. J. Nanomedicine Volume 12, 2001–2019. https://doi.org/10.2147/IJN.S124295

Blanco, E., Shen, H., Ferrari, M., 2015. Principles of nanoparticle design for overcoming biological barriers to drug delivery. Nat. Biotechnol. https://doi.org/10.1038/nbt.3330

Caracciolo, G., Cardarelli, F., Pozzi, D., Salomone, F., Maccari, G., Bardi, G., Capriotti, A.L., Cavaliere, C., Papi, M., Laganà, A., 2013. Selective Targeting Capability Acquired with a Protein Corona Adsorbed on the Surface of 1,2-Dioleoyl-3-trimethylammonium Propane/DNA Nanoparticles. ACS Appl. Mater. Interfaces 5, 13171–13179. https://doi.org/10.1021/am404171h

Caracciolo, G., Farokhzad, O.C., Mahmoudi, M., 2017. Biological Identity of Nanoparticles In Vivo: Clinical Implications of the Protein Corona. Trends Biotechnol. 35, 257–264. https://doi.org/10.1016/j.tibtech.2016.08.011

Chi, J.-T., Chang, H.Y., Haraldsen, G., Jahnsen, F.L., Troyanskaya, O.G., Chang, D.S., Wang, Z., Rockson, S.G., van de Rijn, M., Botstein, D., Brown, P.O., 2003. Endothelial cell diversity revealed by global expression profiling. Proc. Natl. Acad. Sci. 100, 10623–10628. https://doi.org/10.1073/pnas.1434429100

Chithrani, B.D., Ghazani, A.A., Chan, W.C.W., 2006. Determining the Size and Shape Dependence of Gold Nanoparticle Uptake into Mammalian Cells. Nano Lett. 6, 662–668. https://doi.org/10.1021/nl052396o

De Jong, W.H., Hagens, W.I., Krystek, P., Burger, M.C., Sips, A.J.A.M., Geertsma, R.E., 2008. Particle size-dependent organ distribution of gold nanoparticles after intravenous administration. Biomaterials 29, 1912–1919. https://doi.org/10.1016/j.biomaterials.2007.12.037

Ding, B. Sen, Dziubla, T., Shuvaev, V. V., Muro, S., Muzykantov, V.R., 2006. Advanced drug delivery systems that target the vascular endothelium. Mol. Interv.

https://doi.org/10.1124/mi.6.2.7

Ferrari, M., 2005. Cancer nanotechnology: opportunities and challenges. Nat. Rev. Cancer 5, 161–171. https://doi.org/10.1038/nrc1566

Francia, V., Aliyandi, A., Salvati, A., 2018. Effect of the development of a cell barrier on nanoparticle uptake in endothelial cells. Nanoscale 10, 16645–16656. https://doi.org/10.1039/c8nr03171a

Francia, V., Montizaan, D., Salvati, A., 2020. Interactions at the cell membrane and pathways of internalization of nano-sized materials for nanomedicine. Beilstein J. Nanotechnol. 11, 338–353. https://doi.org/10.3762/bjnano.11.25

Francia, V., Yang, K., Deville, S., Reker-Smit, C., Nelissen, I., Salvati, A., 2019. Corona Composition Can Affect the Mechanisms Cells Use to Internalize Nanoparticles. ACS Nano 13, 11107–11121. https://doi.org/10.1021/acsnano.9b03824

Freese, C., Anspach, L., Deller, R.C., Richards, S.J., Gibson, M.I., Kirkpatrick, C.J., Unger, R.E., 2017. Gold nanoparticle interactions with endothelial cells cultured under physiological conditions. Biomater. Sci. 5, 707–717. https://doi.org/10.1039/c6bm00853d

Georgieva, J. V., Kalicharan, D., Couraud, P.-O., Romero, I.A., Weksler, B., Hoekstra, D., Zuhorn, I.S., 2011. Surface Characteristics of Nanoparticles Determine Their Intracellular Fate in and Processing by Human Blood–Brain Barrier Endothelial Cells In Vitro. Mol. Ther. 19, 318–325. https://doi.org/10.1038/mt.2010.236

Gromnicova, R., Kaya, M., Romero, I.A., Williams, P., Satchell, S., Sharrack, B., Male, D., 2016. Transport of Gold Nanoparticles by Vascular Endothelium from Different Human Tissues. PLoS One 11, e0161610. https://doi.org/10.1371/journal.pone.0161610

He, C., Hu, Y., Yin, L., Tang, C., Yin, C., 2010. Effects of particle size and surface charge on cellular uptake and biodistribution of polymeric nanoparticles. Biomaterials 31, 3657–3666. https://doi.org/10.1016/j.biomaterials.2010.01.065

Hirn, S., Semmler-Behnke, M., Schleh, C., Wenk, A., Lipka, J., Schäffler, M., Takenaka, S., Möller, W., Schmid, G., Simon, U., Kreyling, W.G., 2011. Particle size-dependent and surface charge-dependent biodistribution of gold nanoparticles after intravenous administration. Eur. J. Pharm. Biopharm. 77, 407–416. https://doi.org/10.1016/j.ejpb.2010.12.029

Iversen, T.G., Skotland, T., Sandvig, K., 2011. Endocytosis and intracellular transport of nanoparticles: Present knowledge and need for future studies. Nano Today. https://doi.org/10.1016/j.nantod.2011.02.003

Klingberg, H., Loft, S., Oddershede, L.B., Møller, P., 2015. The influence of flow, shear stress and adhesion molecule targeting on gold nanoparticle uptake in human endothelial cells. Nanoscale 7, 11409–11419. https://doi.org/10.1039/c5nr01467k

Kowalski, P.S., Leus, N.G.J., Scherphof, G.L., Ruiters, M.H.J., Kamps, J.A.A.M., Molema, G., 2011. Targeted siRNA delivery to diseased microvascular endothelial cells-Cellular and molecular concepts. IUBMB Life. https://doi.org/10.1002/iub.487

Kowalski, P.S., Lintermans, L.L., Morselt, H.W.M., Leus, N.G.J., Ruiters, M.H.J., Molema, G., Kamps, J.A.A.M., 2013. Anti-VCAM-1 and anti-E-selectin SAINT-O-somes for selective delivery of siRNA into inflammation-activated primary endothelial cells. Mol.

Pharm. 10, 3033–3044. https://doi.org/10.1021/mp4001124

Krump-Konvalinkova, V., Bittinger, F., Unger, R.E., Peters, K., Lehr, H.-A., Kirkpatrick, C.J., 2001. Generation of Human Pulmonary Microvascular Endothelial Cell Lines. Lab. Investig. 81, 1717–1727. https://doi.org/10.1038/labinvest.3780385

Lara, S., Alnasser, F., Polo, E., Garry, D., Lo Giudice, M.C., Hristov, D.R., Rocks, L., Salvati, A., Yan, Y., Dawson, K.A., 2017. Identification of Receptor Binding to the Biomolecular Corona of Nanoparticles. ACS Nano 11, 1884–1893. https://doi.org/10.1021/acsnano.6b07933

Lara, S., Perez-Potti, A., Herda, L.M., Adumeau, L., Dawson, K.A., Yan, Y., 2018. Differential Recognition of Nanoparticle Protein Corona and Modified Low-Density Lipoprotein by Macrophage Receptor with Collagenous Structure. ACS Nano 12, 4930–4937. https://doi.org/10.1021/acsnano.8b02014

Lesniak, A., Fenaroli, F., Monopoli, M.P., Åberg, C., Dawson, K.A., Salvati, A., 2012. Effects of the Presence or Absence of a Protein Corona on Silica Nanoparticle Uptake and Impact on Cells. ACS Nano 6, 5845–5857. https://doi.org/10.1021/nn300223w

Lesniak, A., Salvati, A., Santos-Martinez, M.J., Radomski, M.W., Dawson, K.A., Åberg, C., 2013. Nanoparticle adhesion to the cell membrane and its effect on nanoparticle uptake efficiency. J. Am. Chem. Soc. 135, 1438–1444. https://doi.org/10.1021/ja309812z

Lundqvist, M., Stigler, J., Elia, G., Lynch, I., Cedervall, T., Dawson, K.A., 2008. Nanoparticle size and surface properties determine the protein corona with possible implications for biological impacts. Proc. Natl. Acad. Sci. U. S. A. 105, 14265–14270. https://doi.org/10.1073/pnas.0805135105

Maiorano, G., Sabella, S., Sorce, B., Brunetti, V., Malvindi, M.A., Cingolani, R., Pompa, P.P., 2010. Effects of cell culture media on the dynamic formation of protein-nanoparticle complexes and influence on the cellular response. ACS Nano 4, 7481–7491. https://doi.org/10.1021/nn101557e

Monopoli, M.P., Walczyk, D., Campbell, A., Elia, G., Lynch, I., Baldelli Bombelli, F., Dawson, K.A., 2011. Physical−Chemical Aspects of Protein Corona: Relevance to in Vitro and in Vivo Biological Impacts of Nanoparticles. J. Am. Chem. Soc. 133, 2525–2534. https://doi.org/10.1021/ja107583h

Muro, S., Garnacho, C., Champion, J.A., Leferovich, J., Gajewski, C., Schuchman, E.H., Mitragotri, S., Muzykantov, V.R., 2008. Control of endothelial targeting and intracellular delivery of therapeutic enzymes by modulating the size and shape of ICAM-1-targeted carriers. Mol. Ther. 16, 1450–1458. https://doi.org/10.1038/mt.2008.127

Nel, A.E., Mädler, L., Velegol, D., Xia, T., Hoek, E.M.V., Somasundaran, P., Klaessig, F., Castranova, V., Thompson, M., 2009. Understanding biophysicochemical interactions at the nano-bio interface. Nat. Mater. https://doi.org/10.1038/nmat2442

Parent, R., Durantel, D., Lahlali, T., Sallé, A., Plissonnier, M.-L., DaCosta, D., Lesca, G., Zoulim, F., Marion, M.-J., Bartosch, B., 2014. An immortalized human liver endothelial sinusoidal cell line for the study of the pathobiology of the liver endothelium. Biochem. Biophys. Res. Commun. 450, 7–12. https://doi.org/10.1016/j.bbrc.2014.05.038

Partikel, K., Korte, R., Mulac, D., Humpf, H.U., Langer, K., 2019. Serum type and concentration both affect the protein-corona composition of PLGA nanoparticles.

Beilstein J. Nanotechnol. 10, 1002–1015. https://doi.org/10.3762/BJNANO.10.101

Peer, D., Karp, J.M., Hong, S., Farokhzad, O.C., Margalit, R., Langer, R., 2007. Nanocarriers as an emerging platform for cancer therapy. Nat. Nanotechnol. 2, 751–760. https://doi.org/10.1038/nnano.2007.387

Rejman, J., Oberle, V., Zuhorn, I.S., Hoekstra, D., 2004. Size-dependent internalization of particles via the pathways of clathrin- and caveolae-mediated endocytosis. Biochem. J. 377, 159–169. https://doi.org/10.1042/bj20031253

Ribatti, D., Nico, B., Vacca, A., Roncali, L., Dammacco, F., 2002. Endothelial cell heterogeneity and organ specificity. J. Hematotherapy Stem Cell Res. https://doi.org/10.1089/152581602753448559

Ritz, S., Schöttler, S., Kotman, N., Baier, G., Musyanovych, A., Kuharev, J., Landfester, K., Schild, H., Jahn, O., Tenzer, S., Mailänder, V., 2015. Protein Corona of Nanoparticles: Distinct Proteins Regulate the Cellular Uptake. Biomacromolecules 16, 1311–1321. https://doi.org/10.1021/acs.biomac.5b00108

Sahay, G., Alakhova, D.Y., Kabanov, A. V., 2010. Endocytosis of nanomedicines. J. Control. Release 145, 182–195. https://doi.org/10.1016/j.jconrel.2010.01.036

Salvati, A., Pitek, A.S., Monopoli, M.P., Prapainop, K., Bombelli, F.B., Hristov, D.R., Kelly, P.M., Åberg, C., Mahon, E., Dawson, K.A., 2013. Transferrin-functionalized nanoparticles lose their targeting capabilities when a biomolecule corona adsorbs on the surface. Nat. Nanotechnol. 8, 137–143. https://doi.org/10.1038/nnano.2012.237

Satchell, S.C., Tasman, C.H., Singh, A., Ni, L., Geelen, J., von Ruhland, C.J., O'Hare, M.J., Saleem, M.A., van den Heuvel, L.P., Mathieson, P.W., 2006. Conditionally immortalized human glomerular endothelial cells expressing fenestrations in response to VEGF. Kidney Int. 69, 1633–1640. https://doi.org/10.1038/sj.ki.5000277

Semete, B., Booysen, L., Lemmer, Y., Kalombo, L., Katata, L., Verschoor, J., Swai, H.S., 2010. In vivo evaluation of the biodistribution and safety of PLGA nanoparticles as drug delivery systems. Nanomedicine Nanotechnology, Biol. Med. 6, 662–671. https://doi.org/10.1016/j.nano.2010.02.002

Shapero, K., Fenaroli, F., Lynch, I., Cottell, D.C., Salvati, A., Dawson, K.A., 2011. Time and space resolved uptake study of silica nanoparticles by human cells. Mol. Biosyst. 7, 371–378. https://doi.org/10.1039/c0mb00109k

Shen, Y., Tang, H., Radosz, M., Van Kirk, E., Murdoch, W.J., 2008. PH-responsive nanoparticles for cancer drug delivery. Methods Mol. Biol. 437, 183–216. https://doi.org/10.1007/978-1-59745-210-6_10

Simone, E., Ding, B. Sen, Muzykantov, V., 2009. Targeted delivery of therapeutics to endothelium. Cell Tissue Res. https://doi.org/10.1007/s00441-008-0676-7

Strojan, K., Leonardi, A., Bregar, V.B., Križaj, I., Svete, J., Pavlin, M., 2017. Dispersion of nanoparticles in different media importantly determines the composition of their protein corona. PLoS One 12, e0169552. https://doi.org/10.1371/journal.pone.0169552

Tenzer, S., Docter, D., Kuharev, J., Musyanovych, A., Fetz, V., Hecht, R., Schlenk, F., Fischer, D., Kiouptsi, K., Reinhardt, C., Landfester, K., Schild, H., Maskos, M., Knauer, S.K., Stauber, R.H., 2013. Rapid formation of plasma protein corona critically affects nanoparticle pathophysiology. Nat. Nanotechnol. 8, 772–781.

https://doi.org/10.1038/nnano.2013.181

Waegeneers, N., Brasseur, A., Van Doren, E., Van der Heyden, S., Serreyn, P.J., Pussemier, L., Mast, J., Schneider, Y.J., Ruttens, A., Roels, S., 2018. Short-term biodistribution and clearance of intravenously administered silica nanoparticles. Toxicol. Reports 5, 632–638. https://doi.org/10.1016/j.toxrep.2018.05.004

Wang, C., De Jong, E., Sjollema, K.A., Zuhorn, I.S., 2016. Entry of PIP3-containing polyplexes into MDCK epithelial cells by local apical-basal polarity reversal. Sci. Rep. 6, 21436. https://doi.org/10.1038/srep21436

Weksler, B.B., Subileau, E. a, Perrière, N., Charneau, P., Holloway, K., Leveque, M., Tricoire-Leignel, H., Nicotra, A., Bourdoulous, S., Turowski, P., Male, D.K., Roux, F., Greenwood, J., Romero, I. a, Couraud, P.O., 2005. Blood-brain barrier-specific properties of a human adult brain endothelial cell line. FASEB J. 19, 1872–1874. https://doi.org/10.1096/fj.04-3458fje

Wilhelm, S., Tavares, A.J., Dai, Q., Ohta, S., Audet, J., Dvorak, H.F., Chan, W.C.W., 2016. Analysis of nanoparticle delivery to tumours. Nat. Rev. Mater. 1, 1–12. https://doi.org/10.1038/natrevmats.2016.14

Yang, K., Mesquita, B., Horvatovich, P., Salvati, A., 2020. Tuning liposome composition to modulate corona formation in human serum and cellular uptake. Acta Biomater. 106, 314–327. https://doi.org/10.1016/j.actbio.2020.02.018

Zuhorn, I.S., Kalicharan, D., Robillard, G.T., Hoekstra, D., 2007. Adhesion receptors mediate efficient non-viral gene delivery. Mol. Ther. 15, 946–953. https://doi.org/10.1038/mt.sj.6300139

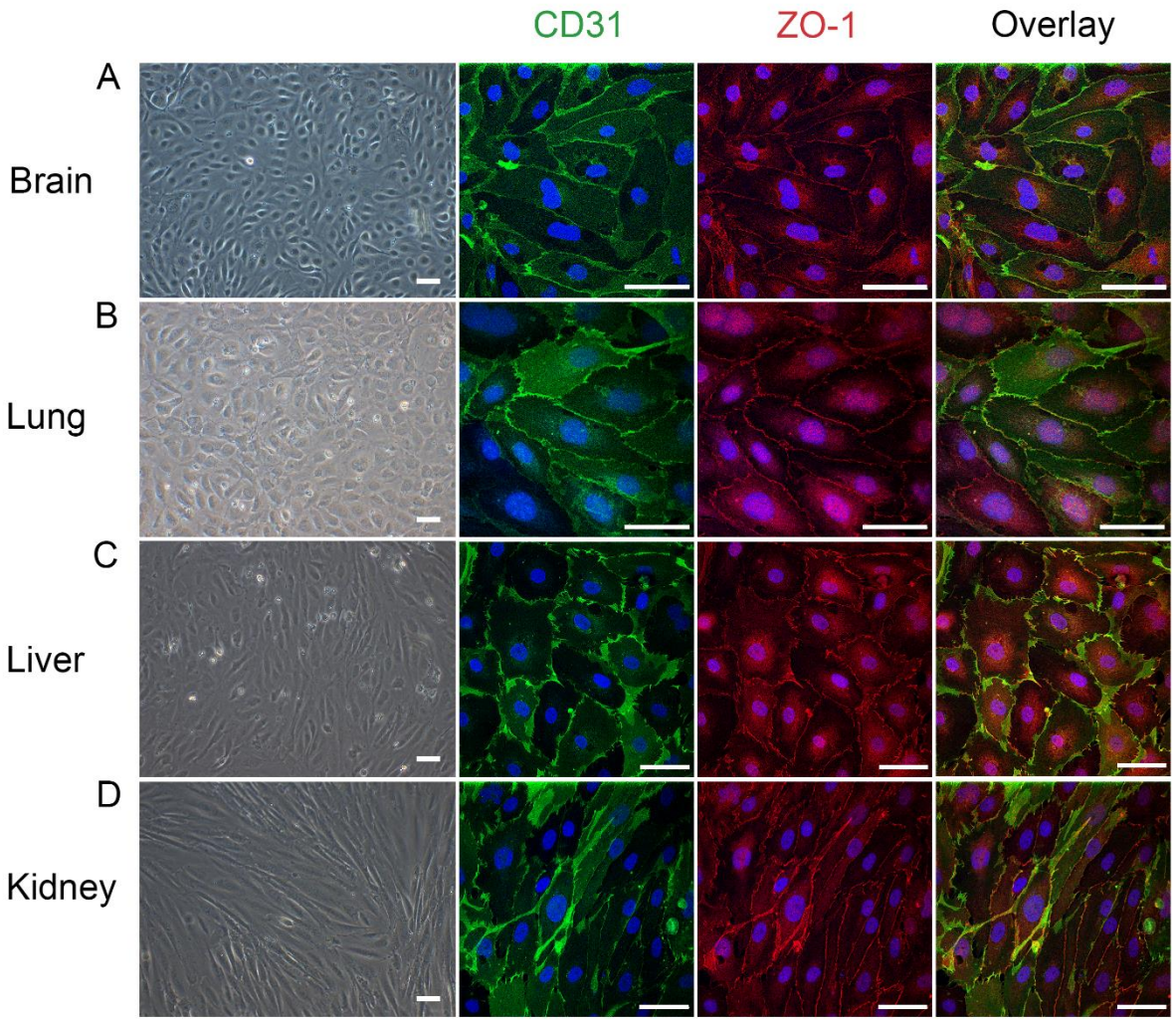

Figure 1. Morphology, ZO-1, and CD31 expression in endothelial barriers derived from different organs. Endothelial barriers were prepared as described in the Methods. Left: light microscopy images of the endothelial barriers (scale bar: 50 μm). Right: confocal images of anti-ZO-1 (red) and anti-CD31 (green) immunostainings. Blue: DAPI stained nuclei (scale bar: 50 μm). (A) hCMEC/D3, (B) HPMEC-ST1.6R, (C) TRP3, and (D) ciGENC cells.

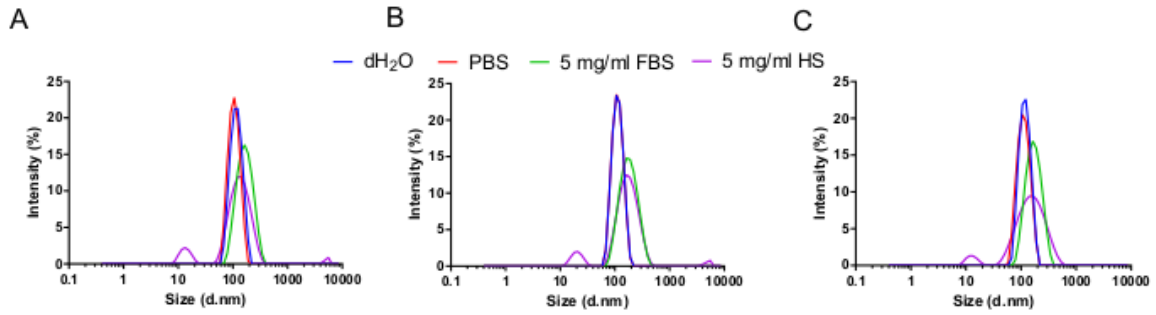

Figure 2. Size distribution by intensity (diameter, d, nm) of 100 nm SiO_2 (A), SiO_2-NH_2 (B), and SiO_2-COOH (C) as obtained by dynamic light scattering (DLS). Silica nanoparticles (100 µg/ml) were dispersed in dH_2O, PBS, and EBM-2 cell culture medium supplemented with 5 mg/ml of FBS or human serum (HS). All nanoparticles remained stable after dispersion in the cell culture medium with serum.

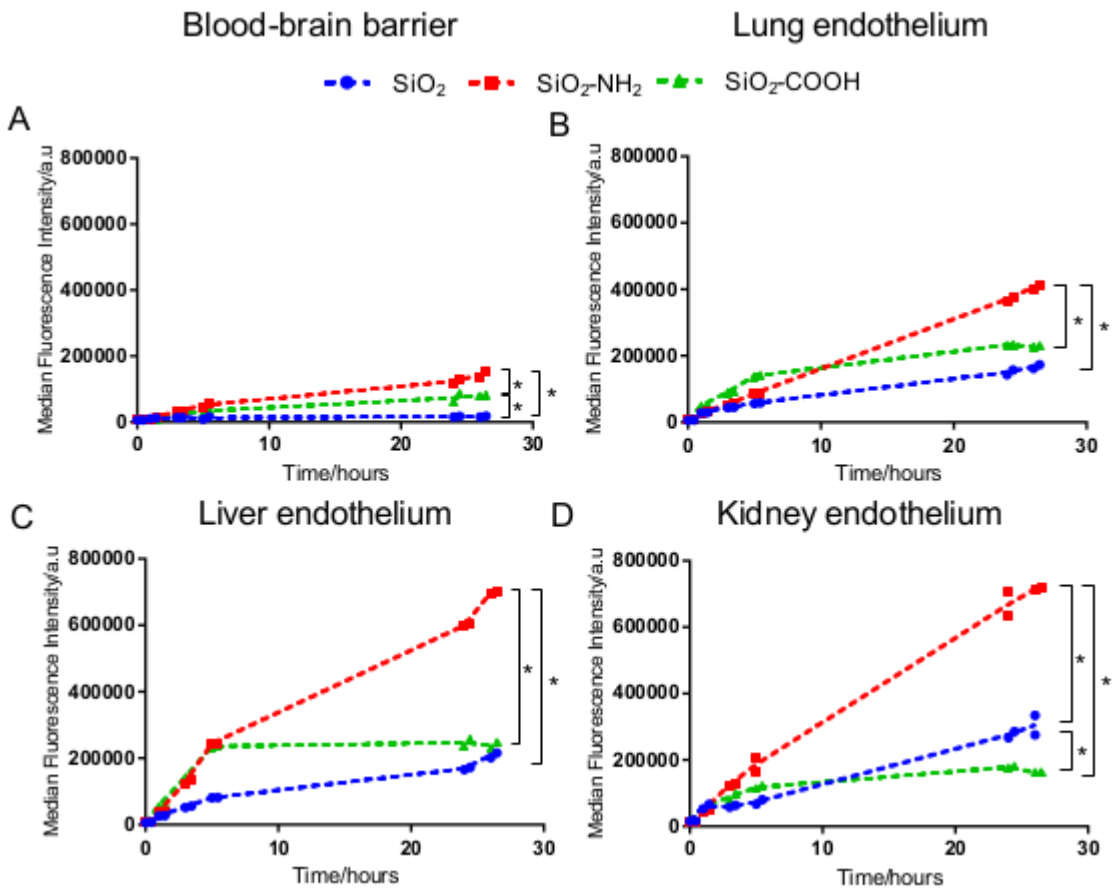

665 **Figure 3.** Nanoparticle uptake levels in endothelial barriers derived from different organs in the presence of bovine serum. Median cell fluorescence intensity as obtained by flow cytometry of hCMEC/D3 (A), HPMEC-ST1.6R (B), TRP3 (C), and ciGENC (D) exposed to different nanoparticles. Endothelial barriers were prepared as described in the Methods and exposed to 50 µg/ml of 100 nm SiO_2, SiO_2-NH_2, or SiO_2-COOH in a cell culture medium supplemented 670 with 5 mg/ml FBS for the indicated times. The median cell fluorescence intensity of two replicate samples is shown, together with their mean (indicated with a line connecting the mean of each time point). The results of an independent replicate experiment are shown in Supplementary Figure S2. For each uptake kinetics, a linear regression two-tailed Student's t-test was applied to compare them (see Section 2.9 for details). Statistically significant 675 differences are indicated with an asterisk. $p \leq 0.05$ was considered significant.

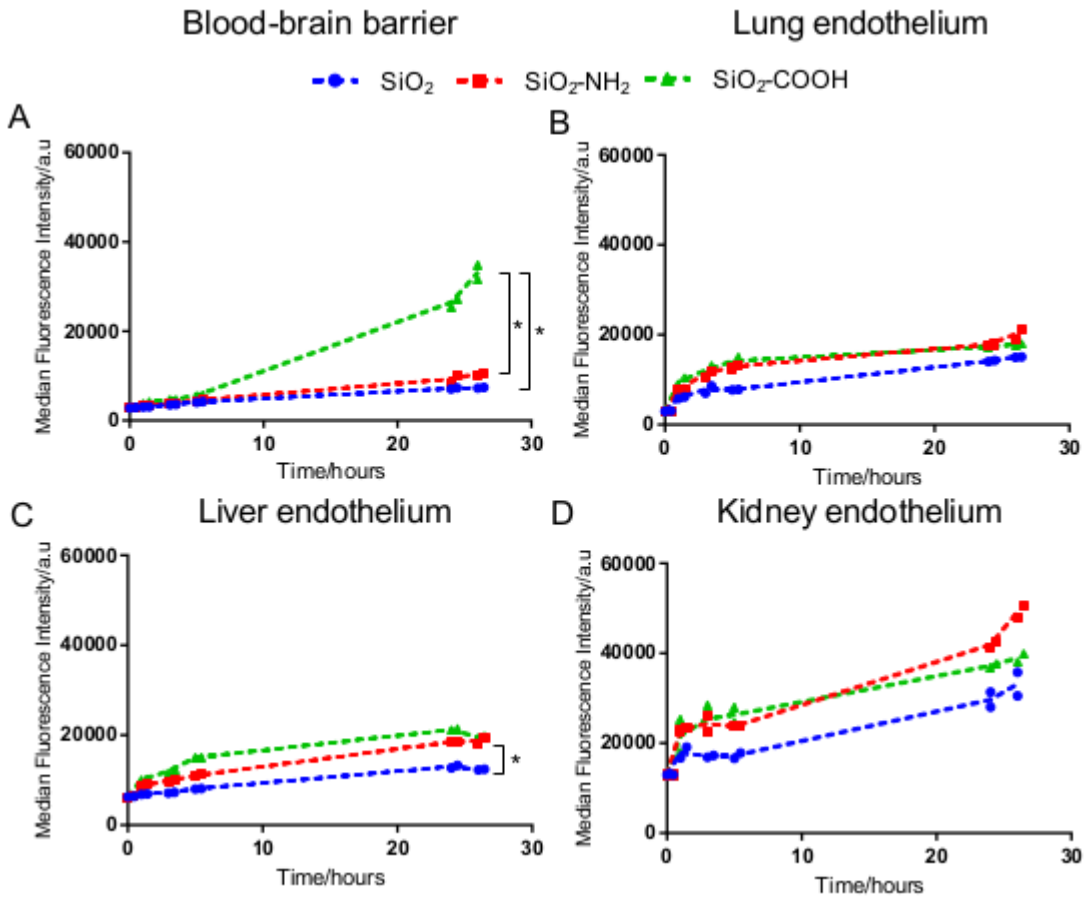

Figure 4. Nanoparticle uptake levels in endothelial cells derived from different organs in the presence of human serum. Median cell fluorescence intensity as obtained by flow cytometry of hCMEC/D3 (A), HPMEC-ST1.6R (B), TRP3 (C), and ciGENC (D) exposed to different nanoparticles. Endothelial barriers were prepared as described in the Methods and exposed to 50 µg/ml 100 nm SiO_2, SiO_2-NH_2, or SiO_2-COOH in a cell culture medium supplemented with 5 mg/ml human serum for the indicated times. The median cell fluorescence intensity of two replicate samples is shown, together with their mean (indicated with a line connecting the mean of each time point). The results of an independent replicate experiment are shown in Supplementary Figure S3. For each uptake kinetics, a linear regression two-tailed Student's t-test was applied to compare them (see Section 2.9 for details). Statistically significant differences are indicated with an asterisk. $p \leq 0.05$ was considered significant.

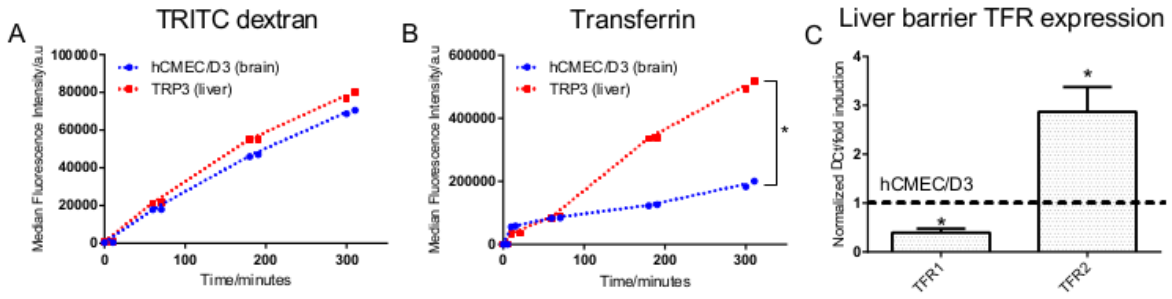

Figure 5. Rates of endocytosis and expression levels of transferrin receptors in liver and brain endothelial barriers. Median cell fluorescence intensity as obtained by flow cytometry of hCMEC/D3 and TRP3 barriers exposed to different fluorescent molecules. Endothelial barriers were prepared as described in the Methods and exposed to 250 µg/ml TRITC dextran 10 kDa in cell culture medium (A) or 10 µg/ml Alexa Fluor546 fluorescently labeled transferrin (B) in serum-free medium for the indicated times. The median cell fluorescence intensity of two replicate samples is shown, together with their mean (indicated with a line connecting the mean of each time point). The results of an independent replicate experiment are shown in Supplementary Figure S4. For each uptake kinetics, a linear regression two-tailed Student's t-test was applied to compare them (see Section 2.9 for details). Statistically significant differences are indicated with an asterisk. $p \leq 0.05$ was considered significant. C: expression levels of genes coding for the transferrin receptors TFR1 and TFR2 in TRP3 in comparison to hCMEC/D3. The results are average and standard deviation over four technical replicates of the fold-change in gene expression levels in TRP3 normalized to the expression levels in hCMEC/D3, calculated as detailed in the Methods (C). An unpaired two-tailed student's t-test was used to determine statistically significant difference compared to the expression level in hCMEC/D3 cells (see Section 2.9 for details). Statistically significant differences are indicated with an asterisk (*$p < 0.05$ n = 4).